JCTC Journal of Chemical Theory and Computation

Article

pubs.acs.org/JCTC

Mechanistic Insights into the Rate-Limiting Step in Purine-Specific Nucleoside Hydrolase

Nanhao Chen,[†,§] Yuan Zhao,[‡,§] Jianing Lu,[‡] Ruibo Wu,*[,†] and Zexing Cao*[,‡]

[†]School of Pharmaceutical Sciences, Sun Yat-sen University, Guangzhou, 510006, People's Republic of China

[‡]State Key Laboratory of Physical Chemistry of Solid Surfaces and Fujian Provincial Key Laboratory of Theoretical and Computational Chemistry, College of Chemistry and Chemical Engineering, Xiamen University, Xiamen, 360015, People's Republic of China

Supporting Information

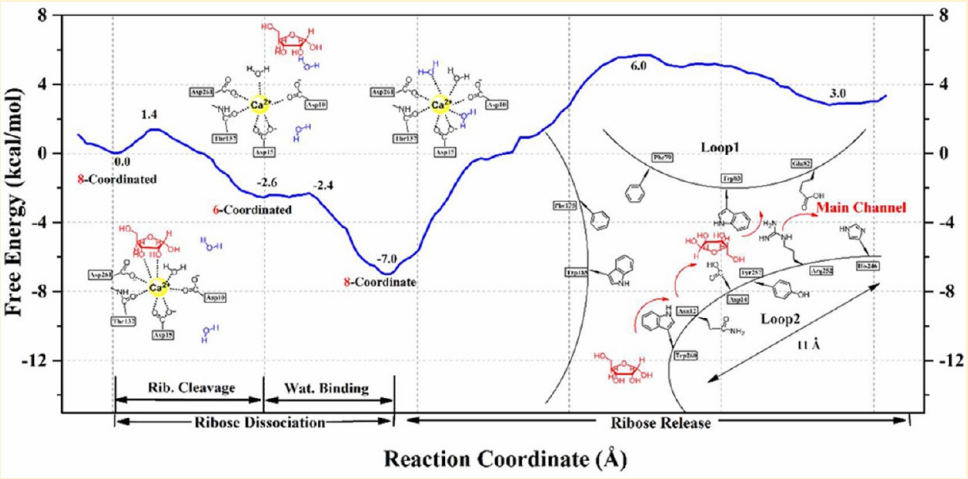

ABSTRACT: A full enzymatic catalysis cycle in the inosine−adenosine−guanosine specific nucleoside hydrolase (IAG-NH) was assumed to be comprised of four steps: substrate binding, chemical reaction, base release, and ribose release. Nevertheless, the mechanistic details for the rate-limiting step of the entire enzymatic reaction are still unknown, even though the ribose release was likely to be the most difficult stage. Based on state-of-the-art quantum mechanics and molecular mechanics (QM/MM) molecular dynamics (MD) simulations, the ribose release process can be divided into two steps: "ribose dissociation" and "ribose release". The "ribose dissociation" includes "cleavage" and "exchange" stages, in which a metastable 6-fold intermediate will recover to an 8-fold coordination shell of Ca^{2+} as observed in *apo*- IAG-NH. Extensive random acceleration molecular dynamics and MD simulations have been employed to verify plausible release channels, and the estimated barrier for the rate-determining step of the entire reaction is 13.0 kcal/mol, which is comparable to the experimental value of 16.7 kcal/mol. Moreover, the gating mechanism arising from loop1 and loop2, as well as key residues around the active pocket, has been found to play an important role in manipulating the ribose release.

INTRODUCTION

The purine-specific nucleoside hydrolases (NHs) play a key role in the purine pathway involved in the N-glycosidic bond hydrolysis of purine ribonucleoside (see Figure 1).[1−3] It is essential for parasites to produce purine through the purine pathway, because of their lack of *de novo* purines synthesis,[4−10] and thus it becomes one attractive antiparasitic target.[11,12] So far, many transition-state analogues have been designed as the NHs inhibitors.[13,14] As one subgroup of NHs, IAG-NH prefers hydrolyzing inosine, adenosine, and guanosine.[15] Although several crystal structures of IAG-NH have been determined in the past decades,[16−21] only two complete structures (PDB ID: 2FF2, 3EPW)[19,21] were solved, revealing two important and very flexible loops around the active pocket (loop1: residue 75−85; loop2: residue 244−258). (See Table S1 in the Supporting Information and Figure 1).

Experimentally, a four-step kinetic model (substrate binding, chemical reaction, base release, and ribose release) was proposed for the catalytic mechanism by IAG-NH,[22−24] and the "ribose release" was assumed to be the rate-limiting step,[18,23] as shown in Figure 1. Nevertheless, the detailed mechanistic insight into the rate-limiting step is still unknown. Considering that the ribose might be bidentately coordinated with the center Ca^{2+} after the "base release", it would be better to further divide the "ribose release" into two stages: ribose

Received: January 18, 2015

DOI: 10.1021/acs.jctc.5b00045
J. Chem. Theory Comput. XXXX, XXX, XXX−XXX

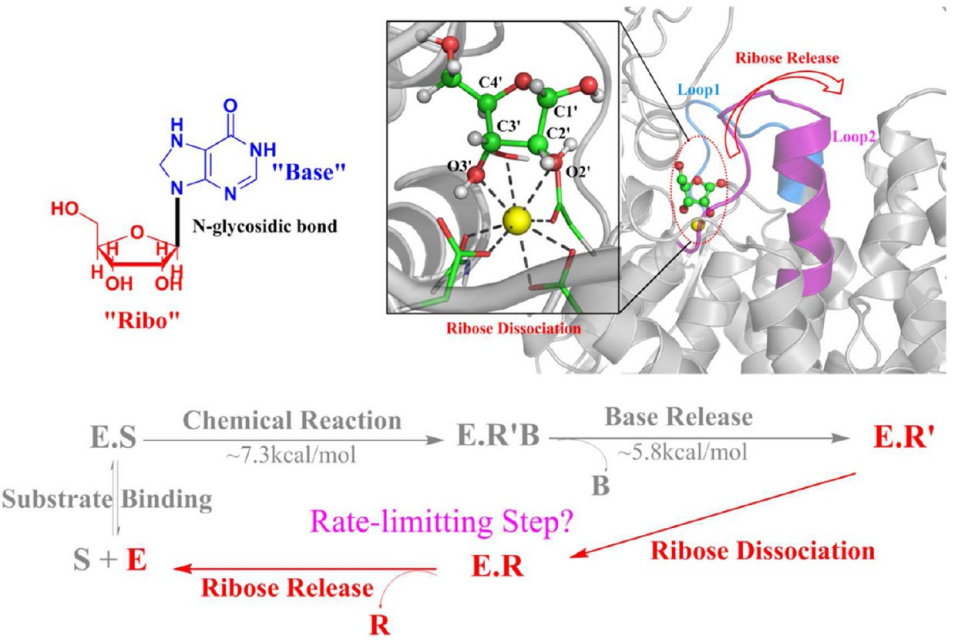

Figure 1. Substrate and protein structure of IAG-NH and the four-step kinetic model. Herein, the coordination of the calcium is highlighted and the barriers of steps that we studied before are also marked. (Legend: E, enzyme; S, substrate; R, ribose; B, base.)

dissociation and release (see Figure 1). We note that the experimental rate constant is ~3.6 s^{-1} for the procedure after base release,[23] which suggests a barrier of ~16.7 kcal/mol for this enzymatic reaction. Recently, the chemical reaction and base release procedures had been explored theoretically, and the predicted barriers for the chemical step and base release are only ~7 kcal/mol[25] and ~5.6 kcal/mol,[26] respectively. These results lend further support to the experimental inference that the rate-limiting step would be subsequent to the base release. However, the exact rate-limiting step (ribose dissociation or ribose release) for the entire catalytic cycle in IAG-NH is still not clear.

Herein, the "ribose dissociation" stage has been elaborately studied by combined quantum mechanics and molecular mechanics (QM/MM) simulations, which represent one state-of-the-art tool to study the enzyme catalysis (involving the bond breakage and formation)[27−29] at the electronic level. The random acceleration molecular dynamics (RAMD)[30,31] then were performed to identify the possible ribose release channel. Finally, the "ribose release" stage has been identified to be the rate-limiting step by classical MD with umbrella sampling, which are widely used in featuring the dynamical behaviors of biological macromolecules at the atomic level.[32]

METHOD

QM/MM MD Simulations. The initial structure (see Figure S1 in the Supporting Information) was obtained from the last window of the base release.[26] Both chains were maintained in the simulations, because of the large accessible surface area buried in the dimer interface.[21] Herein, the AMBER GAFF force field[33] for ribose in both chains and the AMBER99SB force field[34] for protein were employed. The system was solvated in one rectangular box of TIP3P water molecules,[35] and the entire system includes ~93 000 atoms. All the MD preparations were generated by the *tleap* program in AMBER12[36] and the previous molecular dynamics (MD) protocol[26] (see the details in the Supporting Information) was adopted to get a stable ER′ state (namely, the final state after base release; see Figure 1).

The last snapshot of MM MD simulations was chosen as the initial QM/MM model (see Figure S3(a) in the Supporting Information) by deleting the water molecules beyond 25 Å from the Ca ion of the first chain. Herein, the residues and ribose coordinated with the Ca ion and the water molecules within 7 Å around Ca^{2+} (in order to include the possible waters which would substitute the ribose and finally coordinate with the Ca ion) are considered as the QM region (69 atoms in total, see Figure S2(a) in the Supporting Information). All the atoms in QM part are treated with the B3LYP functional using the 6-31G(d) basis set and atoms in the MM part are described by the AMBER99SB force field. The improved pseudo-bond approach[37−39] was used to deal with the QM/MM boundary. The 12 and 18 Å cutoffs were used for the van der Waals and electrostatic interactions, respectively.

The detailed procedures are shown in Figure S2(b) in the Supporting Information, and here the QM/MM simulations were composed of three steps. At first, one concerted RC (RC2, cleavage concerted with exchange) was considered (see Figure S3 in the Supporting Information). However, the resulting relative energy continued to increase and the water molecules would not coordinate with the Ca ion with RC2. The stepwise RCs then were chosen, and the sum of the distances $d_{O2'-Ca}$ and $d_{O3'-Ca}$ was chosen as the reaction coordinate (RC1; see details in Figure S3 in the Supporting Information) to describe the cleavage process, while the reaction coordinate (RC) was set as the sum of the d_{OW2-Ca} and d_{OW3-Ca} (RC3), to elucidate the exchange process. For these two processes, both started with the minimum energy path (MEP), which was mapped by the reaction coordinates driving method.[40] Then, 500 ps MD simulations were utilized to equilibrate the MM part with the QM subsystem constrained. Finally, the *ab initio* QM/MM MD simulations combined with the umbrella sampling[41] were carried out. Each window was equilibrated for 5 ps simulations and then another 15 ps MD simulations for

DOI: 10.1021/acs.jctc.5b00045
J. Chem. Theory Comput. XXXX, XXX, XXX−XXX

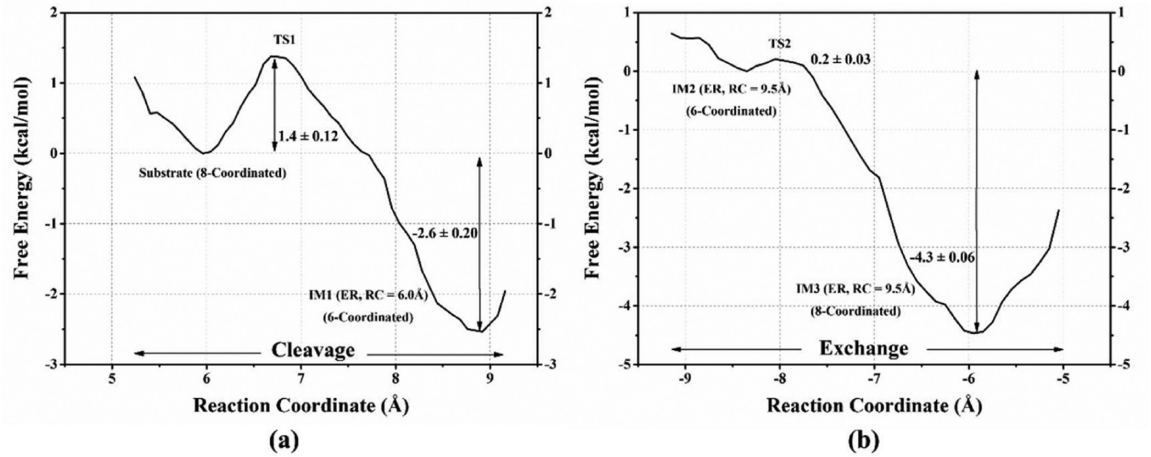

Figure 2. Free-energy profiles of the ribose dissociation, which is divided into coordinative bond (a) "cleavage" and (b) "exchange" (two additional waters would coordinate to Ca^{2+} again) stages. Herein, the cleavage part and exchange part are discontinuous, because of an additional active pocket geometry arrangement from one intermediate state (IM1) to another (IM2). Unfortunately, it is not feasible to map out the free-energy profile from IM1 to IM2, because of the limitation of QM/MM modeling, with so complicated reaction coordination combination. Nevertheless, in the aspect of kinetics, the ribose is solvated by lots of water so that it is not hard for the following ribose release and the water entering into the Ca^{2+} coordination shell. In the view of thermodynamics, the two substituted water molecules will take the place of the ribose (see Figure 3, r1 in IM1 is nearly the same as the d1 in IM2, and the water molecule would form one hydrogen bond with Asp261, which is similar to the hydrogen bond between the OH3′ atom of the ribose and the carbonyl of Asp261) to reconstruct the very similar Ca−O coordination interaction. Meanwhile, the "exchange" part actually occurs after "cleavage" part and coupled with the subsequent ribose release procedure. The SD values were estimated statistically (see details in Figure S4 in the Supporting Information).

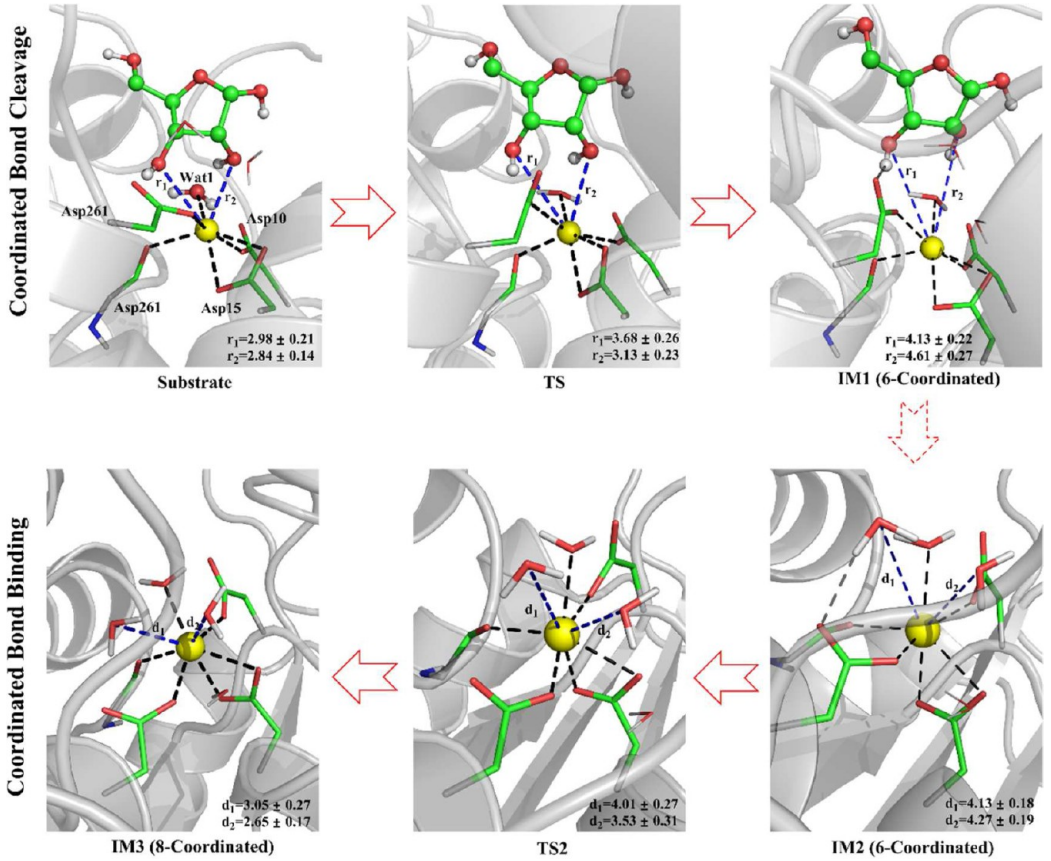

Figure 3. Representative structures during the ribose dissociation. The distances between the ligands (ribose and waters) and the calcium are highlighted.

the statistics. During the simulations, the water exchange between the solvent and the QM area was not observed (at least no exchange in the 30 ps), because of the strong hydrogen bond network between these waters and the coordinated residues. All the QM/MM simulations were performed by the modified Q-Chem[42] and Tinker[43] programs. The following free

DOI: 10.1021/acs.jctc.5b00045
J. Chem. Theory Comput. XXXX, XXX, XXX−XXX

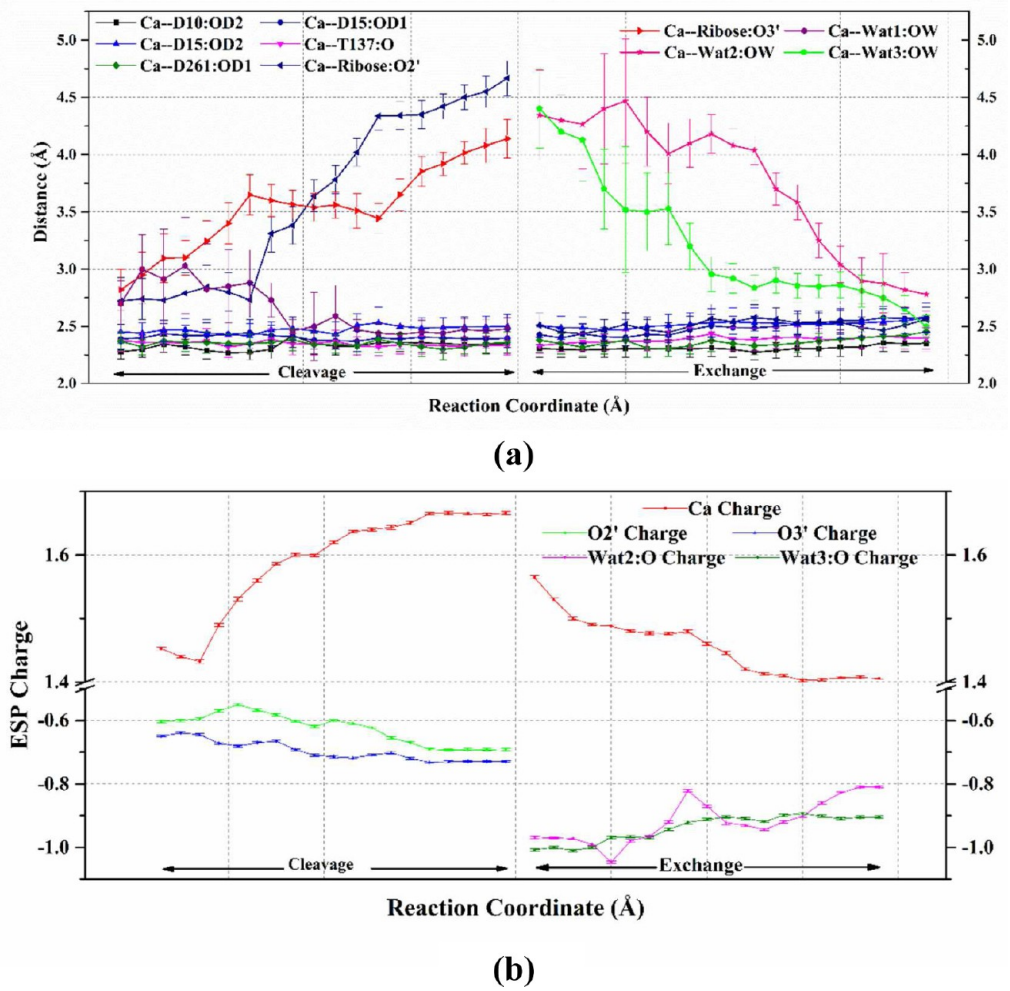

Figure 4. (a) Coordination bonds and (b) ESP charge distribution evolution along the ribose dissociation procedure.

energy analysis was performed by using the weighted histogram analysis method (WHAM).[44,45]

Classical MD Simulations. In order to determine the plausible channels for the ribose release, the RAMD simulations[46] were carried out by the NAMD 2.9 software.[47,48] A constant force with random orientation was applied to the centroid of the ligand. When this ligand moves away out of the threshold distance, this direction would be preserved and another conventional MD simulation would be implemented to equilibrate this structure. Otherwise, another new random direction will be set to determine the ligand release pathway. Herein, the random accelerations of 0.50, 0.30, and 0.20 kcal/g/Å were employed for the ribose and the threshold distance values of 0.002 and 0.004 Å were set for each acceleration. All simulations were applied to the alternating 50 steps of RAMD and 100 steps of classical MD protocols and all combinations were repeated three times. Finally, the obtained 18 RAMD trajectories have been employed to determine the most plausible channel. The classical MM MD simulations, combined with umbrella sampling, then were carried out to get the free-energy profile. The distance between the Ca ion and the C4′ atom was chosen as the reaction coordinate, and it varies from 6.0 Å to 13.0 Å in MD simulations for all windows separated by 0.4 Å. Each window was simulated for at least 8 ns after equilibrium. Finally, the potential of the mean force along the RC was calculated by WHAM[44,45] program.

RESULTS AND DISCUSSIONS

I. Dissociation of Ribose Bound to Ca^{2+}. The free-energy profiles during the "ribose dissociation" process are delineated in Figure 2. Apparently, the cleavage of the dative bonds between Ca^{2+} and ribose (O2′ and O3′) are facile and nearly spontaneous only with a barrier of 1.4 kcal/mol and an exothermicity of 2.5 kcal/mol (Figure 2a). The representative active sites along this reaction are depicted in Figure 3. At the ER′ state, the two oxygen atoms of the ribose are still coordinated with the Ca ion, even though both dative bonds are remarkably weakened (the bonding distances are 2.98 and 2.84 Å, respectively). The average separation for other chelation bonds is ∼2.31 Å, as shown in Figure 4a. We note that the cleavage of both dative bonds occurs asynchronously, in which the O3′−Ca^{2+} bond breaking is prior to the O2′−Ca^{2+} bond, as shown in Figures 3 and Figure 4a. At the TS1 state, the O3′ is 3.68 Å away from Ca^{2+}, and is completely dissociated from Ca^{2+}. The cleavage of the O3′−Ca^{2+} bond is facilitated by the help of Asp261, which always forms a very strong hydrogen bond with the O3′ atom from the ER′ state to the TS1 state. In contrast, the distance increase of O2′−Ca^{2+} becomes faster than that of O3′−Ca^{2+} (O2′−Ca^{2+}: from 3.13 to 4.61; O3′−Ca^{2+}: from 3.68 to 4.13) after the TS1 state, yielding the IM state, in which there are more positive ESP charges on the calcium ion (increases from ∼1.43 to ∼1.67) and more negative charges on O2′ and O3′ (see Figure 4).

DOI: 10.1021/acs.jctc.5b00045
J. Chem. Theory Comput. XXXX, XXX, XXX−XXX

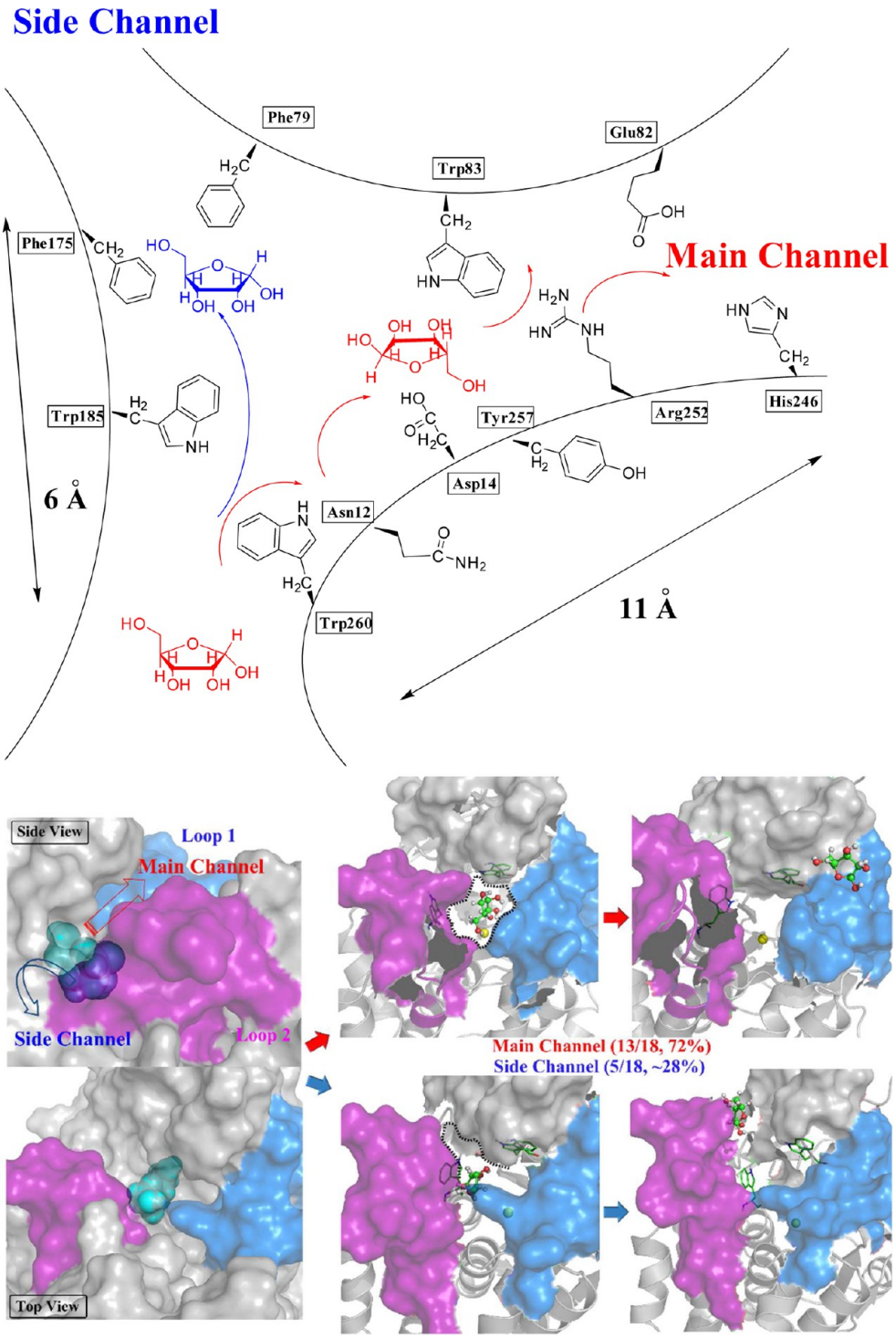

Figure 5. Two plausible channels for ribose release and their possibility on the basis of RAMD simulations.

Although the coordinate number of Ca ion change to be 6-fold at the IM1 state, the coordination shell was well-maintained, even after additional 20 ps nonrestrained QM/MM MD simulations at this state. Considering that the Ca ion should be eight-coordinated with another two water molecules in the *apo*- IAG-NH (PDB ID: 1HOZ), naturally we can assume that two water molecules would replace the position of O2′ and O3′ during the ribose release to promote the catalytic cycle to the original *apo*-state. Since there are so many water molecules around the dissociated ribose (see details in Figure S5 in the Supporting Information), the subsequent ligand exchange is possible. Thus, at the beginning stage of the ribose release, followed by the conformation rearrangement and water/ribose movement (see Figure 3, as well as Figure S5 in the Supporting Information), two water molecules would approach the Ca ion gradually from the IM1 state to the IM2 state as well as the TS2 state (see Figure 4a, IM1 is located around ribose release RC = 6.8 Å and IM2 is located at RC ≈ 9.5 Å). By comparison of IM1 and IM2, the obvious difference between these two states is the number of water molecules

DOI: 10.1021/acs.jctc.5b00045
J. Chem. Theory Comput. XXXX, XXX, XXX−XXX

around the Ca ion, which increase distinctly in IM2 (see Figures S5(c) and S5(d) in the Supporting Information). There is still 6-fold coordinated Ca at both IM1 and IM2 states, while it would become 7-coordinated at the TS2 state. Similar to the geometry situation at the cleavage step, the coordination between protein and the Ca ion is quite stable at the exchange step (see Figure 4a). For the ESP charges of the QM atoms, the high positive charges of the Ca ion would bring higher coordination ability and make it easier to recover the 8-coordinated state. From the IM2 state to the IM3 state, the charge transfer from the two coordinated water molecules to the calcium is observed distinctly (see the "exchange" part in Figure 4b). Moreover, as shown in Figure 2b, it would be very easy to bind with other two water molecules, because of the negligible barrier and exothermicity of 4.5 kcal/mol after the ribose leaving away from the bottom of the active site, to evolve to the stable IM3 state, whose coordination structure of Ca^{2+} is very similar to that in *apo*-IAG NH (PDB ID: 1HOZ). These results suggest that both IM1 and IM2 are metastable.

Accordingly, it is spontaneous for the recovery of the 8-fold coordination shell of Ca^{2+} in *apo*-IAG-NH from ER′ to the ER state by the "cleavage" and "exchange" stages, with the presence of two metastable intermediates IM1 and IM2. As Figure 2 shows, the entire ribose dissociation process experiences a barrier of ∼1.4 kcal/mol, with an energy release of ∼7 kcal/mol, and thus it absolutely is not the rate-limiting step.

II. Release of Ribose from the Active Pocket. According to the RAMD trajectories, two possible ribose release pathways have been found. As shown in Figure 5, one is "main channel" which is surround by loop 1 and loop 2, and the other is "side channel" which is close to loop 2 and another loop (residues: 175−184). The main channel has a dominant share of release trajectories (∼72%), which is also responsible for the base release.[26] Only five trajectories (∼28%) are contributed by the side channel. The following intriguing question arises here: Why does the ribose release prefer the deeper main channel (∼11 Å) but not the side channel (∼6 Å). We note that there are many polar residues (such as Asn12, Asp14, Glu82, His246, Arg252, and so on) around the main channel, while there are rich nonpolar residues around the side channel (such as Trp185, Trp260, Phe79, and Phe175), as shown in Figure 5. Furthermore, we found that the main channel is wider than the side channel (see Figure 5).

To clarify the thermodynamic and kinetic details of the ribose release, the free-energy profiles along the release process are also calculated by classical MD with umbrella sampling (see Figure 6). The predicted barrier for the ribose release is ∼13 kcal/mol, which is significantly higher than the barriers of other steps (as summarized in Figure 1). Since this barrier is close to the experimental value of ∼16.7 kcal/mol,[23] we proposed that the ribose release is the rate-limiting step for the entire catalytic cycle in the IAG-NH. Although the last ribose release step is endothermic by 10 kcal/mol, it is exothermic for the entire enzymatic reaction composed of the substrate binding, chemical step, and product release (∼3 kcal/mol, as shown in Figure 7). Based on the entire free-energy profiles for the enzyme catalysis cycle, the product state of the hydrolysis reaction is the most stable ligand-binding state, which indicates that it may be an effective way to mimic the hydrolysis product state to inhibit the enzyme activity with high binding affinity thermodynamically. Moreover, the structural modification to prevent the ligand release would be helpful for increase of the "drug-target" resident times, which is relative to the critical drug

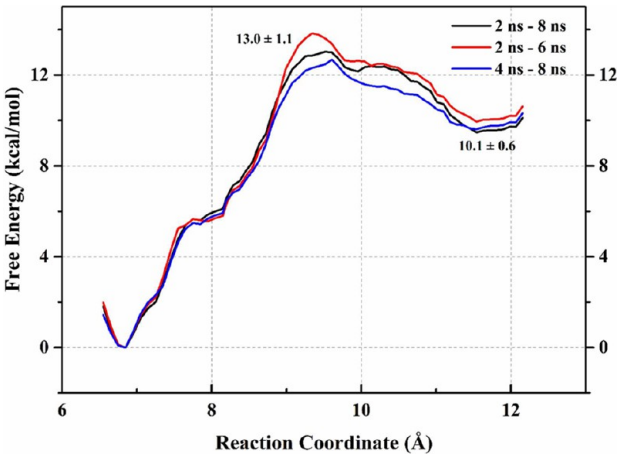

Figure 6. Free-energy profiles for the ribose release. RC is defined as the distance of the C4′−Ca^{2+} bond. The SD values were estimated based on the three free-energy profiles selected from different time scales.

binding kinetics.[49,50] Therefore, it is guidable for drug design to further understand the functional roles of the loop, as well as key residues involving the ribose release.

There are many aromatic residues, such as, Trp83, Trp185, Tyr255, Tyr256, Trp260, and so on, around the bottom of the channel;thus, how does a strong polar molecule like ribose penetrate through this area? Herein, classical MD simulations with umbrella sampling reveal that the conformation of ribose would flip over. As shown in Figure 8, the side chain of Trp83 is like a lid to cover the pocket at the initial step. When the ribose moves around RC = 9.4 Å along the channel, because of the polar outside and the nonpolar inside, the ribose would flip over gradually. At that time, numerous water molecules flow into the pocket around the ribose and the side chain of Trp83 opens up the avenue. As a result, the hydroxyl groups would form a more-complicated hydrogen bond network with the residues directly or indirectly. At RC = 9.4 Å, the guanidine group of Arg252 forms the hydrogen bond with the ribose through the water molecule, and the ribose has almost accomplished the flipping movement. Afterward, another residue of loop2, Tyr257, forms the indirect hydrogen bond with the ribose. At RC = 10.5 Å, the ribose forms the hydrogen bond with the Arg252 directly and would be exposed to the solvent. As for the process from RC = 10.5 Å to RC = 11.5 Å, the ribose would be hindered significantly by this strong polar group (hydrogen bonds), increasing the resident time of the ribose; thus, it is unfavorable for the ribose release. It is quite consistent with the R252A mutant experiment that the ribose release would be promoted significantly. Besides, the Y257A mutant would also have positive impact on the ribose release process. Therefore, we proposed that lack of the polar group (hydrogen bond interaction) and large aromatic group (space hinder effect) would accelerate the ribose release and promote the solvent flowing into the pocket, which would increase the contact between the ribose and the solvent.

Distinguished conformation changes of the two key loops (loop1 and loop2) are observed during the ribose release. As the conformation recovery of the Trp83 would occur from the substrate to the transition state, the secondary structure, the helix part (residues 78−82), would unwind to loop at the same time. Herein, the RMSF of loop1 exhibits a significant increase during the ribose release (see details in Figure S6 in the

DOI: 10.1021/acs.jctc.5b00045
J. Chem. Theory Comput. XXXX, XXX, XXX−XXX

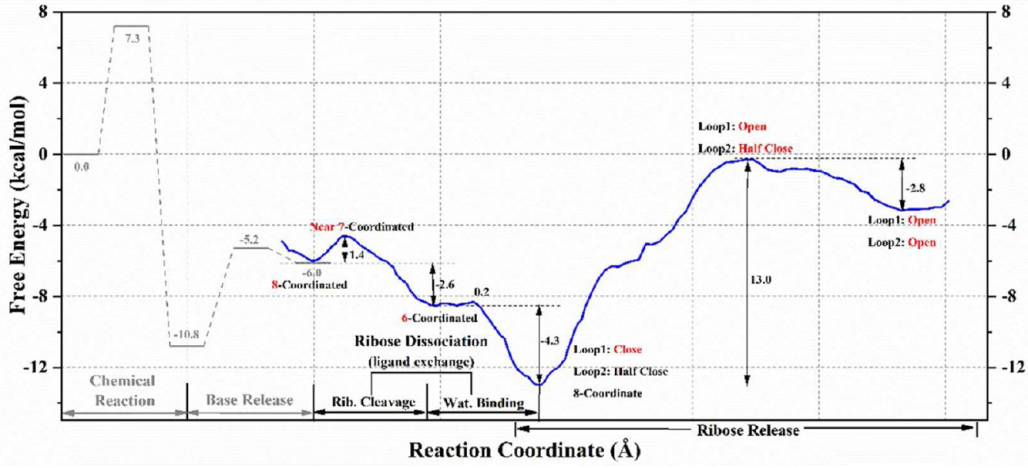

Figure 7. Entire free-energy profiles for the IAG-NH catalysis. The states of the loop motif are highlighted in red. As for the states IM1 and IM2, the differences between these two states are also reflected by the PMF of the ribose release (where IM1 is located at RC = 6.5 Å and IM2 is located at RC = 9.5 Å).

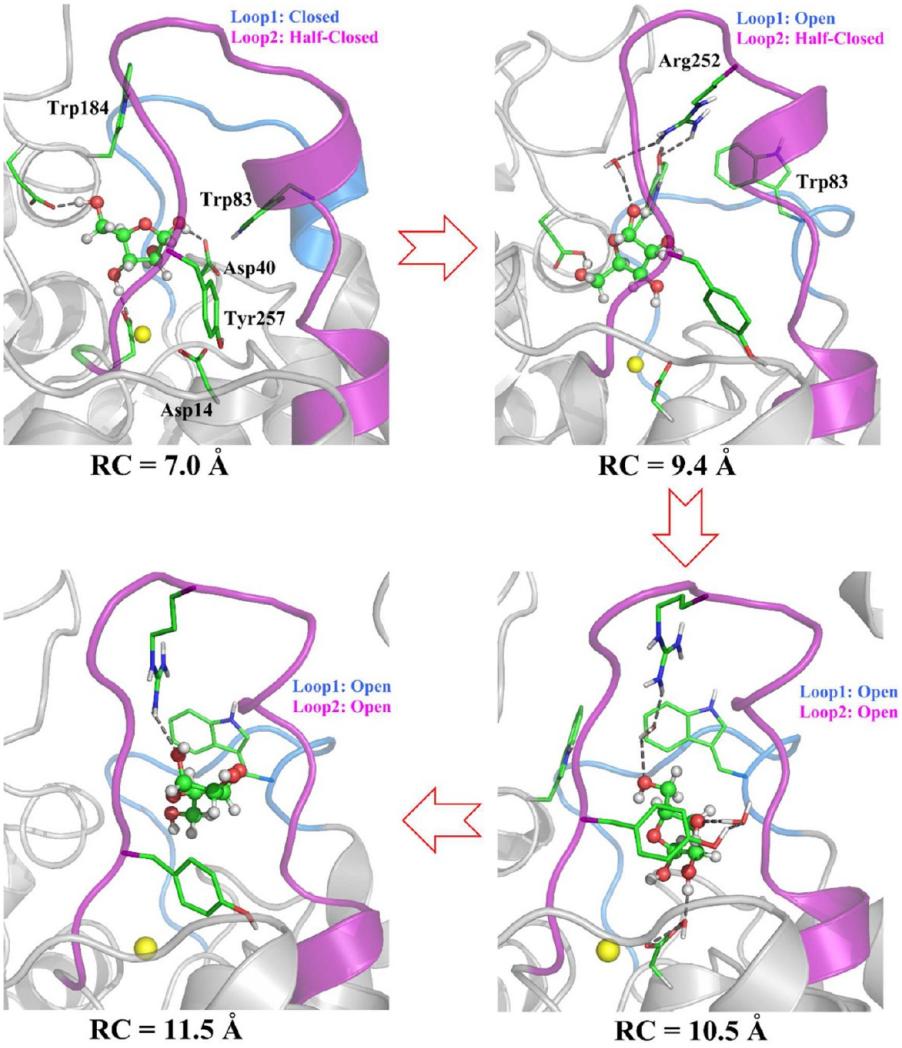

Figure 8. Representative structures along the ribose release from the main channel under the classical MD simulations with umbrella sampling. Loop1 is colored marine and loop2 is colored purple. The ribose is shown by a ball-and-stick model, while the residues are shown by a stick model. Clearly, the helix part of loop1 would unwind from the state of RC = 7.0 Å to RC = 9.4 Å. And loop2 would change from a half-closed state to an open state after the transition state (RC = 9.4 Å).

DOI: 10.1021/acs.jctc.5b00045
J. Chem. Theory Comput. XXXX, XXX, XXX−XXX

Supporting Information), showing that the conformation of loop1 changes from a closed state to an open state, as shown in Figure 8. Regarding to loop2, because of the indirect hydrogen bond between Tyr257 and ribose (see in Figure 8), its conformation would change from a half-closed state to an open state after RC = 9.4 Å. According to the overlap of two crystal structures in Figure S7 in the Supporting Information, two key residues control the conformation change of loop2, namely, Trp242 and Tyr257. The side chain of the former residue was proven to have flipped over during the base release, leading to the loop2 conformation change from the closed state to the half-closed state in our previous study and trigger the following ribose release process.[26] The later one, Tyr257, forms the indirect hydrogen bond with the ribose through the phenolic hydroxyl group, which flips the orientation of side chain from inside to outside, which coincides with the crystal structure.

CONCLUSION

Herein, we have elucidated the ribose dissociation and release involved in the IAG-NH catalytic reaction theoretically. It reveals that the ribose dissociation includes "cleavage" and "exchange" stages. At the "cleavage" stage, one six-coordinated metastable intermediate is observed due to the polar ribose may prevent the coordination of subsequent water molecules to Ca^{2+}. Then, followed by the release of this polar ribose from the main channel and away from the bottom of the active pocket, the metastable six-coordinated state of Ca^{2+} will recover to be 8-fold coordination shell as observed in *apo*-IAG-NH experimentally. Furthermore, the ribose release is identified to be the rate-limiting step of the entire catalytic cycle with the barrier of ∼13 kcal/mol, and the flip of ribose and the motion of loop from "close" to "open" around the active pocket are involved in this process, and the flip of the ribose are essential in the rate-limiting step. Meanwhile, the increase of the water molecules in pocket leads a more flexible loop1 and the ribose release activates another controller of loop2, Tyr257, which regulates the conformational change from "closed" to "open" for loop2. These findings shed lights on future experiments in site-directed mutagenesis and designing higher affinity, as well as better binding-kinetic-behavior NH inhibitors.

ASSOCIATED CONTENT

Supporting Information

The available IAG-NH crystal structures, all protocols in simulations and conformational change details during the ribose release. The Supporting Information is available free of charge on the ACS Publications website at DOI: 10.1021/acs.jctc.5b00045.

AUTHOR INFORMATION

Corresponding Authors

*E-mail: wurb3@mail.sysu.edu.cn (R. Wu).
*E-mail: zxcao@xmu.edu.cn (Z. Cao).

Author Contributions

§N. Chen and Y. Zhao contributed equally to this work.

Notes

The authors declare no competing financial interest.

ACKNOWLEDGMENTS

This work was supported by the National Natural Science Foundation of China (Nos. 21203257 and 21272289), Pearl River S&T Nova Program of Guangzhou (No. 2014J2200062), and the Ministry of Science and Technology (No. 2011CB808504). We also thank the National Supercomputing Center in Shenzhen and Guangzhou for providing the computational resources. We also thank Dr. Shenglong Wang at NYU-ITS for his kind help.

REFERENCES

(1) Versees, W.; Steyaert, J. *Curr. Opin. Struct. Biol.* **2003**, *13*, 731.
(2) el Kouni, M. H. *Pharmacol. Ther.* **2003**, *99*, 283.
(3) Downie, M. J.; Kirk, K.; Mamoun, C. B. *Eukaryotic Cell* **2008**, *7*, 1231.
(4) Ogawa, J.; Takeda, S.; Xie, S. X.; Hatanaka, H.; Ashikari, T.; Amachi, T.; Shimizu, S. *Appl. Environ. Microbiol.* **2001**, *67*, 1783.
(5) Cui, L.; Rajasekariah, G. R.; Martin, S. K. *Gene* **2001**, *280*, 153.
(6) Kurtz, J. E.; Exinger, F.; Erbs, P.; Jund, R. *Curr. Genet.* **2002**, *41*, 132.
(7) Petersen, C.; Møller, L. B. *J. Biol. Chem.* **2001**, *276*, 884.
(8) Ribeiro, J. M.; Valenzuela, J. G. *Insect Biochem. Mol. Biol.* **2003**, *33*, 13.
(9) Versees, W.; Van Holsbeke, E.; De Vos, S.; Decanniere, K.; Zegers, I.; Steyaert, J. *Acta Crystallogr., Sect. D: Biol. Crystallogr.* **2003**, *59*, 1087.
(10) Pelle, R.; Schramm, V. L.; Parkin, D. W. *J. Biol. Chem.* **1998**, *273*, 2118.
(11) Miles, R. W.; Tyler, P. C.; Evans, G. B.; Furneaux, R. H.; Parkin, D. W.; Schramm, V. L. *Biochemistry* **1999**, *38*, 13147.
(12) Ranquin, A.; Versees, W.; Meier, W.; Steyaert, J.; Van Gelder, P. *Nano Lett.* **2005**, *5*, 2220.
(13) Evans, G. B.; Furneaux, R. H.; Greatrex, B.; Murkin, A. S.; Schramm, V. L.; Tyler, P. C. *J. Med. Chem.* **2008**, *51*, 948.
(14) Goeminne, A.; Berg, M.; McNaughton, M.; Bal, G.; Surpateanu, G.; Van der Veken, P.; De Prol, S.; Versees, W.; Steyaert, J.; Haemers, A.; Augustyns, K. *Bioorg. Med. Chem.* **2008**, *16*, 6752.
(15) Parkin, D. W. *J. Biol. Chem.* **1996**, *271*, 21713.
(16) Versees, W.; Decanniere, K.; Pelle, R.; Depoorter, J.; Brosens, E.; Parkin, D. W.; Steyaert, J. *J. Mol. Biol.* **2001**, *307*, 1363.
(17) Versees, W.; Decanniere, K.; Van Holsbeke, E.; Devroede, N.; Steyaert, J. *J. Biol. Chem.* **2002**, *277*, 15938.
(18) Versees, W.; Loverix, S.; Vandemeulebroucke, A.; Geerlings, P.; Steyaert, J. *J. Mol. Biol.* **2004**, *338*, 1.
(19) Versees, W.; Barlow, J.; Steyaert, J. *J. Mol. Biol.* **2006**, *359*, 331.
(20) Vandemeulebroucke, A.; De Vos, S.; Van Holsbeke, E.; Steyaert, J.; Versees, W. *J. Biol. Chem.* **2008**, *283*, 22272.
(21) Versees, W.; Goeminne, A.; Berg, M.; Vandemeulebroucke, A.; Haemers, A.; Augustyns, K.; Steyaert, J. *Biochim. Biophys. Acta* **2009**, *1794*, 953.
(22) Vandemeulebroucke, A.; Versees, W.; Steyaert, J.; Barlow, J. N. *Biochemistry* **2006**, *45*, 9307.
(23) Vandemeulebroucke, A.; Versees, W.; De Vos, S.; Van Holsbeke, E.; Steyaert, J. *Biochemistry* **2003**, *42*, 12902.
(24) Barlow, J. N.; Steyaert, J. *Biochim. Biophys. Acta* **2007**, *1774*, 1451.
(25) Wu, R.; Gong, W.; Liu, T.; Zhang, Y.; Cao, Z. *J. Phys. Chem. B* **2012**, *116*, 1984.
(26) Chen, N.; Ge, H.; Xu, J.; Cao, Z.; Wu, R. *Biochim. Biophys. Acta* **2013**, *1834*, 1117.
(27) Chen, N. H.; Zhou, J. W.; Li, J. B.; Xu, J.; Wu, R. B. *J. Chem. Theory Comput.* **2014**, *10*, 1109.
(28) Shi, Y. W.; Zhou, Y. Z.; Wang, S. L.; Zhang, Y. K. *J. Phys. Chem. Lett.* **2013**, *4*, 491.
(29) Rooklin, D. W.; Lu, M.; Zhang, Y. K. *J. Am. Chem. Soc.* **2012**, *134*, 15595.
(30) Ludemann, S. K.; Lounnas, V.; Wade, R. C. *J. Mol. Biol.* **2000**, *303*, 813.
(31) Ludemann, S. K.; Lounnas, V.; Wade, R. C. *J. Mol. Biol.* **2000**, *303*, 797.
(32) Dror, R. O.; Dirks, R. M.; Grossman, J. P.; Xu, H.; Shaw, D. E. *Annu. Rev. Biophys.* **2012**, *41*, 429.

DOI: 10.1021/acs.jctc.5b00045
J. Chem. Theory Comput. XXXX, XXX, XXX−XXX

(33) Wang, J.; Wolf, R. M.; Caldwell, J. W.; Kollman, P. A.; Case, D. A. *J. Comput. Chem.* **2004**, *25*, 1157.
(34) Duan, Y.; Wu, C.; Chowdhury, S.; Lee, M. C.; Xiong, G.; Zhang, W.; Yang, R.; Cieplak, P.; Luo, R.; Lee, T.; Caldwell, J.; Wang, J.; Kollman, P. *J. Comput. Chem.* **2003**, *24*, 1999.
(35) Jorgensen, W. L.; Chandrasekhar, J.; Madura, J. D.; Impey, R. W.; Klein, M. L. *J. Chem. Phys.* **1983**, *79*, 926.
(36) Case, D. A.; Darden, T. A.; Cheatham, T. E., III; Simmerling, C. L.; Wang, J.; Duke, R. E.; Luo, R.; Walker, R. C.; Zhang, W.; Merz, K. M.; Roberts, B.; Hayik, S.; Roitberg, A.; Seabra, G.; Swails, J.; Goetz, A. W.; Kolossváry, I.; Wong, K. F.; Paesani, F.; Vanicek, J.; Wolf, R. M.; Liu, J.; Wu, X.; Brozell, S. R.; Steinbrecher, T.; Gohlke, H.; Cai, Q.; Ye, X.; Wang, J.; Hsieh, M. J.; Cui, G.; Roe, D. R.; Mathews, D. H.; Seetin, M. G.; Salomon-Ferrer, R.; Sagui, C.; Babin, V.; Luchko, T.; Gusarov, S.; Kovalenko, A.; Kollman, P. A. *AMBER 12*; University of California: San Francisco, CA, 2012.
(37) Zhang, Y.; Lee, T. S.; Yang, W. *J. Chem. Phys.* **1999**, *110*, 46.
(38) Chen, X.; Zhang, Y.; Zhang, J. Z. *J. Chem. Phys.* **2005**, *122*, 184105.
(39) Zhang, Y. *Theor. Chem. Acc.* **2006**, *116* (Special Issue of New Perspectives in Theoretical Chemistry).
(40) Zhang, Y.; Liu, H.; Yang, W. *J. Chem. Phys.* **2000**, *112*, 3483.
(41) Torrie, G. M.; Valleau, J. P. *J. Comput. Phys.* **1977**, *23*, 187.
(42) Shao, Y.; Molnar, L. F.; Jung, Y.; Kussmann, J.; Ochsenfeld, C.; Brown, S. T.; Gilbert, A. T.; Slipchenko, L. V.; Levchenko, S. V.; O'Neill, D. P.; DiStasio, R. A., Jr.; Lochan, R. C.; Wang, T.; Beran, G. J.; Besley, N. A.; Herbert, J. M.; Lin, C. Y.; Van Voorhis, T.; Chien, S. H.; Sodt, A.; Steele, R. P.; Rassolov, V. A.; Maslen, P. E.; Korambath, P. P.; Adamson, R. D.; Austin, B.; Baker, J.; Byrd, E. F.; Dachsel, H.; Doerksen, R. J.; Dreuw, A.; Dunietz, B. D.; Dutoi, A. D.; Furlani, T. R.; Gwaltney, S. R.; Heyden, A.; Hirata, S.; Hsu, C. P.; Kedziora, G.; Khalliulin, R. Z.; Klunzinger, P.; Lee, A. M.; Lee, M. S.; Liang, W.; Lotan, I.; Nair, N.; Peters, B.; Proynov, E. I.; Pieniazek, P. A.; Rhee, Y. M.; Ritchie, J.; Rosta, E.; Sherrill, C. D.; Simmonett, A. C.; Subotnik, J. E.; Woodcock, H. L., 3rd; Zhang, W.; Bell, A. T.; Chakraborty, A. K.; Chipman, D. M.; Keil, F. J.; Warshel, A.; Hehre, W. J.; Schaefer, H. F., 3rd; Kong, J.; Krylov, A. I.; Gill, P. M.; Head-Gordon, M. *Phys. Chem. Chem. Phys.* **2006**, *8*, 3172.
(43) Ponder, J. W. *TINKER, Software Tools for Molecular Design*, Version 4.2; Washington University School of Medicine: St. Louis, MO, 2004.
(44) Kumar, S.; Bouzida, D.; Swendsen, R. H.; Kollman, P. A.; Rosenberg, J. M. *J. Comput. Chem.* **1992**, *13*, 1011.
(45) Souaille, M.; Roux, B. *Comput. Phys. Commun.* **2001**, *135*, 40.
(46) Vashisth, H.; Abrams, C. F. *Biophys. J.* **2008**, *95*, 4193.
(47) Phillips, J. C.; Braun, R.; Wang, W.; Gumbart, J.; Tajkhorshid, E.; Villa, E.; Chipot, C.; Skeel, R. D.; Kale, L.; Schulten, K. *J. Comput. Chem.* **2005**, *26*, 1781.
(48) Jiang, W.; Phillips, J. C.; Huang, L.; Fajer, M.; Meng, Y.; Gumbart, J. C.; Luo, Y.; Schulten, K.; Roux, B. *Comput. Phys. Commun.* **2014**, *185*, 908.
(49) Zhang, R. M.; Monsma, F. *Expert Opin. Drug Discovery* **2010**, *5*, 1023.
(50) Zhou, J.; Li, M.; Chen, N.; Wang, S.; Luo, H.; Zhang, Y.; Wu, R. *ACS Chem. Biol.* **2015**, *10*, 687−692.

DOI: 10.1021/acs.jctc.5b00045
J. Chem. Theory Comput. XXXX, XXX, XXX−XXX